



In situ tensile deformation of Fe-rich metallic glass at elevated temperatures using hard X-ray diffraction

J. Bednarcik^{a,*}, S. Michalik^b, H. Franz^a

^a Deutsches Elektronen-Synchrotron DESY, Notkestraße 85, D-22603 Hamburg, Germany

^b Institute of Physics, Faculty of Science, P.J. Safarik University in Kosice, Park Angelinum 9, 041 54 Kosice, Slovakia

ARTICLE INFO

Article history:

Received 31 July 2010

Received in revised form

30 November 2010

Accepted 1 December 2010

Available online 10 December 2010

Keywords:

Metallic glasses

X-ray diffraction

Deformation

ABSTRACT

The present work focuses on the study of the mechanical properties of the $\text{Fe}_{72.5}\text{Cu}_1\text{Nb}_2\text{Mo}_2\text{Si}_{15.5}\text{B}_7$ metallic glass using in situ hard X-ray diffraction techniques. In situ tensile deformation tests provided detailed information about the mechanical properties of the investigated Fe-based metallic glass. Analyzing series of two-dimensional XRD patterns in reciprocal space yields strain tensor components of the amorphous alloy providing insight about its deformation mechanisms. Comparing tensile tests performed at different temperatures indicates that the deformation mechanism gradually changes from purely elastic to completely plastic regime. The Poisson ratio ν of the investigated alloy increases with increasing deformation temperature however the fracture strength σ_f shows opposite behavior.

© 2010 Elsevier B.V. All rights reserved.

1. Introduction

The disordered nature of the structural arrangement in amorphous metallic alloys gives rise to advantageous magnetic, electronic and mechanical properties. Compared with crystalline counterparts, metallic glasses (MGs) have some superior properties, such as high yield strength, hardness, large elastic limit, high fracture toughness and corrosion resistance, and hence are considered as promising engineering materials [1,2]. For the majority of the known MGs, the plastic strain at room temperature is very limited even under compression, resulting from pronounced shear localization and work softening. The lack of plasticity makes MGs prone to catastrophic failure in load-bearing conditions and restricts their application. High-energy X-ray diffraction (XRD) has proven to be a suitable tool to describe the local atomic structure of the metallic glasses [3]. It was recently demonstrated that high-energy X-ray scattering can be used to measure the elastic strain under compression [4,5] and tension [6,7].

The main objective of this work was to follow in situ tensile deformation of Fe-rich soft magnetic metallic glass using high-energy X-ray diffraction. The special emphasis was placed at the deformation behavior at elevated temperatures (but still below the crystallization temperature of the investigated alloy) with the aim to experimentally observe the transition from elastic to plastic deformation.

2. Experimental procedures

Amorphous alloys with nominal composition of $\text{Fe}_{72.5}\text{Cu}_1\text{Nb}_2\text{Mo}_2\text{Si}_{15.5}\text{B}_7$ (at.%) in the shape of $30\ \mu\text{m}$ thin and 9 mm wide ribbons were prepared by single-roller melt spinning technique. A differential scanning calorimeter (NETZSCH DSC 404C) was used to detect the crystallization behavior of as-prepared ribbons under a continuous argon flow at a heating rate of $20\ ^\circ\text{C}/\text{min}$. The thermomagnetic curve was traced at a heating rate of $10\ ^\circ\text{C}/\text{min}$ using a Faraday magnetic balance. In situ tensile experiments using high-energy photon beam (100 keV) were performed at the wiggler beamline BW5 of the positron storage ring DORIS (Hamburg, Germany). The specimens were strained under tension using a test rig from Kamrath and Weiss GmbH allowing to achieve a maximum load of 5 kN. The test rig was further equipped with the resistance ceramic heater covering the temperature range between room temperature and $700\ ^\circ\text{C}$. The temperature uncertainty was $\pm 5\ ^\circ\text{C}$. After loading the sample into the test rig it was embedded in a protective box so that heating could be realized under Ar protective atmosphere. The protective box had two windows covered with Kapton foil thus allowing X-ray diffraction experiments in a transmission geometry. The diffracted photons were collected up to maximum wave vector transfer $q = 165\ \text{nm}^{-1}$ ($q = 4\pi\sin\theta/\lambda$) using an imaging plate detector MAR345 (2300×2300 pixels, each pixel having size of $150 \times 150\ \mu\text{m}^2$) carefully aligned orthogonal to the X-ray beam. Sample-to-detector distance and detector tilt were determined from diffraction patterns obtained from a LaB_6 (NIST 660a) standard reference material.

The strain determination of bulk metallic glasses from X-ray diffraction data is based on concepts previously reported by Poulsen et al. [4]. The symmetric circular diffraction pattern is characterized with respect to the polar coordinates (s, η). In our experiment $\eta = 0^\circ$ and $\eta = 90^\circ$ refer to longitudinal (tensile) and transversal directions, respectively. By dividing the η -range of 0 to 2π into 36 segments, one obtains symmetrized intensity distributions

$$I_i(q, \eta_i) = \int_{\eta_i - \pi/36}^{\eta_i + \pi/36} [I(q, \eta) + I(q, \eta + \pi)] d\eta \quad (1)$$

* Corresponding author.

E-mail address: jozef.bednarcik@desy.de (J. Bednarcik).

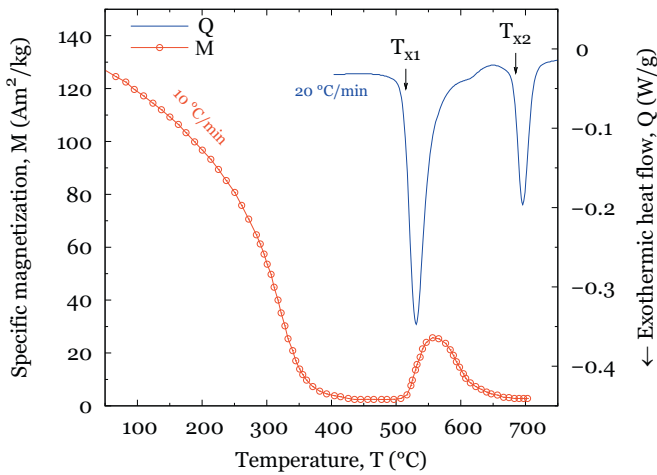


Fig. 1. Thermomagnetic and DSC curves for amorphous $\text{Fe}_{72.5}\text{Cu}_1\text{Nb}_2\text{Mo}_2\text{Si}_{15.5}\text{B}_7$ ribbons. Primary and secondary crystallization events are depicted by arrows.

with $\eta_i = (i-1)\pi/18$, $i = 1 \dots 36$, where the amplitude of wave-vector transfer $q = q(s)$ is defined by

$$q(s) = \frac{4\pi}{\lambda} \sin \left[\frac{1}{2} \arctg \left(\frac{s}{D} \right) \right] \quad (2)$$

in which λ denotes the wavelength, D refers to the sample-to-detector distance and s represents the distance from the origin of the polar coordinate system. Symmetrized intensity distributions as described by Eq. (1) were calculated using the software package FIT2D [8]. The procedure was repeated for all diffraction patterns acquired at different loads thus yielding the set of symmetrized distributions $I_i(q, \eta_i, \sigma)$ where σ refers to the corresponding stress. For each $I_i(q, \eta_i, \sigma)$ the shift in position of the principal diffuse peak, $q_1(\eta_i, \sigma)$, was determined with respect to the unloaded situation, $q_1(\eta_i, \sigma = 0)$. The relative change in the position of the first peak upon applying an external stress defines the strain

$$\varepsilon(\eta_i, \sigma) = \frac{q_1(\eta_i, \sigma = 0) - q_1(\eta_i, \sigma)}{q_1(\eta_i, \sigma)} \quad (3)$$

(with $i = 1 \dots 36$), which is angular dependent. The angular variation of the strain can be fitted to the following expression:

$$\varepsilon(\eta, \sigma) = \varepsilon_{11} \cos^2 \eta - \varepsilon_{12} \sin \eta \cos \eta + \varepsilon_{22} \sin^2 \eta, \quad (4)$$

which yields axial (ε_{11}), tangential (ε_{22}) and in-plane shear (ε_{12}) strain tensor components for the plane perpendicular to the incoming X-ray beam.

3. Results and discussion

The room temperature XRD measurements confirmed the amorphous nature of ribbons in the as-quenched state. As can be seen from the thermomagnetic curve presented in Fig. 1, the investigated alloy maintains its ferromagnetic order up to Curie point ($T_C = 325^\circ\text{C}$) and becomes paramagnetic above that temperature. Since the primary crystallization results in the formation of the ferromagnetic Fe_3Si phase with DO_3 structure, its presence can be also seen on the thermomagnetic curve as a small hump whose onset perfectly matches primary crystallization T_{X1} . The decrease of the magnetization observed above 550°C is due to the ferromagnetic–paramagnetic transition of the Fe_3Si phase which has a Curie temperature of 584°C . DSC curve presented in Fig. 1 reveals two-step crystallization process with onset temperatures of $T_{X1} = 516^\circ\text{C}$ and $T_{X2} = 688^\circ\text{C}$.

To ensure that the investigated alloy does not crystallize during deformation we limited the deformation temperature to 420°C , which is roughly 100°C below the primary crystallization T_{X1} ($=516^\circ\text{C}$). The tensile deformation tests were performed at the temperatures 25, 350, 385 and 420°C . Each tensile test started on a “fresh” 50 mm long piece of the ribbon with adjusting the desired temperature at zero stress. The temperature was then kept constant over the whole period of the deformation test.

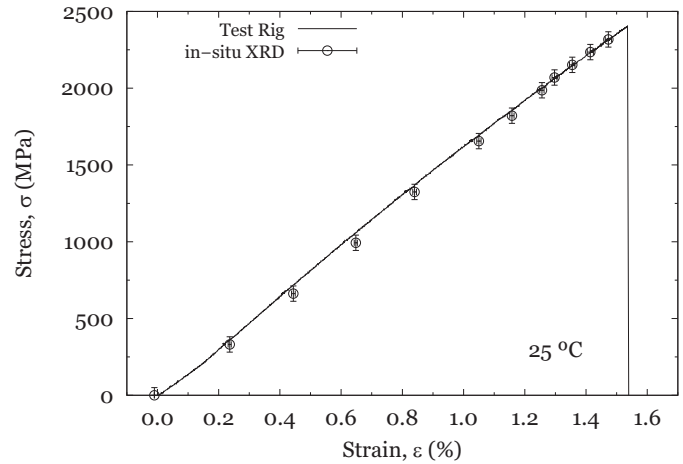


Fig. 2. Comparison of the tensile deformation curves measured at room temperature using a conventional test rig (full line) and in situ XRD (open circles).

Fig. 2 shows tensile stress–strain curves measured at room temperature using a conventional test rig and approach based on the analysis of the two-dimensional XRD patterns. One can observe perfect agreement between the two different methods. Furthermore a linear relation between stress and strain indicates that the investigated alloy deforms elastically at room temperature. It is interesting to note that this regime has been shown to include microplastic events [9]. The fracture strength σ_f , maximum tensile strain ε_{max} and Young modulus E are 2400 MPa, 1.51% and 158 GPa, respectively. In addition the XRD based technique allows simultaneous strain measurement in the transversal direction so one can evaluate the Poisson ratio ν directly. The Poisson ratio ν for the sample deformed at room temperature is 0.26. Another advantage of this technique lays in the fact that it allows observation of the fine structural modifications occurring on the atomic level when deforming metallic glass [5,7].

Fig. 3 shows the stress–strain curves observed in longitudinal (tensile) ε_{11} and transversal ε_{22} directions at the different temperatures. Rather good agreement between conventional test rig measurements and in situ XRD experiments can be observed. One can clearly see that increasing deformation temperature implies decreasing of the fracture strength σ_f of the investigated alloy. Furthermore it is readily seen that increasing the deformation temperature causes the stress–strain curves to deviate from the linear

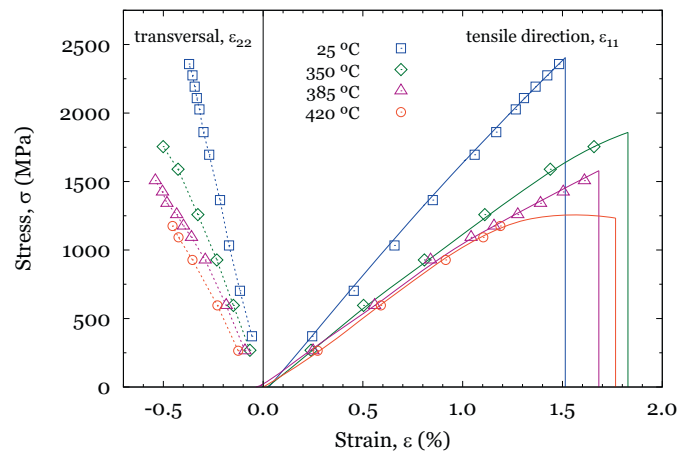


Fig. 3. Comparison of the stress–strain curves observed in longitudinal (tensile) ε_{11} and transversal ε_{22} directions at different temperatures. Open symbols represent values obtained by XRD while full lines correspond to the measurements performed using a test rig.

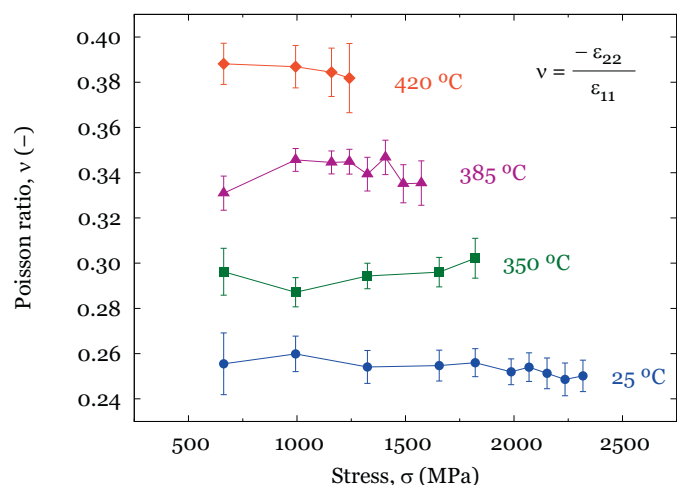


Fig. 4. Temperature–stress behavior of the Poisson ratio ν evaluated from the deformation curves obtained by in situ XRD presented in Fig. 3.

Table 1

Poisson ratio ν , fracture strength σ_f and maximum tensile strain ε_{\max} derived from the tensile stress–strain curves of the alloy deformed at different temperatures T .

T (°C)	ν	σ_f (MPa)	ε_{\max} (%)
25	0.26	2400	1.51
350	0.30	1900	1.83
385	0.34	1600	1.68
420	0.39	1200	1.77

relation. This behavior means that the fraction of plastic deformation progressively increases when deforming amorphous alloy at elevated temperatures. The extent of plastic deformation is pronounced in case of the deformation test performed at 420 °C. Since the heater slightly moved to the side and hence completely blocked the incoming X-ray beam, no XRD data are available within the zone of plastic deformation. Nevertheless the data obtained from the test rig show that after reaching the strain of 1.3% the sample deformed at 420 °C completely yields. Fig. 4 shows the temperature–stress behavior of the Poisson ratio ν evaluated from the deformation curves obtained by in situ XRD. It is apparent from the data shown in Fig. 4 that the Poisson ratio ν increases with increasing defor-

mation temperature. One may conclude that the XRD data, which were obtained below the yielding stress, already reveal the growing extent of the plastic deformation processes as the temperature of deformation is increased. Table 1 summarizes the values of the Poisson ratio ν , fracture strength σ_f and maximum tensile strain ε_{\max} derived from the tensile stress–strain curves of the alloy deformed at the different temperatures.

4. Conclusions

In situ tensile X-ray diffraction experiments on amorphous $\text{Fe}_{72.5}\text{Cu}_1\text{Nb}_2\text{Mo}_2\text{Si}_{15.5}\text{B}_7$ alloy provided data about its mechanical properties. Tracing the position of the principal diffuse peak we obtained microscopic tensile stress–strain curves. The obtained results are in a good agreement with conventional test rig measurements (at least up to the yielding stress). Performing tensile tests at higher temperatures changes the overall deformation response of the amorphous alloy. The extent of the plastic deformation increases with increasing deformation temperature. The Poisson ratio ν of the investigated alloy also increases with increasing temperature, however, the fracture strength σ_f shows opposite behavior.

Acknowledgements

This research was partly supported by the Zhejiang University–Helmholtz cooperation fund. S.M. gratefully acknowledges financial support he received through the DAAD fellowship.

References

- [1] A. Inoue, *Acta Mater.* 48 (2000) 279.
- [2] W.L. Johnson, *MRS Bull.* 24 (1999) 42.
- [3] T. Egami, S.J.L. Billinge, *Underneath the Bragg Peaks: Structural analysis of complex materials*, Pergamon Press/Elsevier, Oxford, England, 2003.
- [4] H.F. Poulsen, J.A. Wert, J. Neuefeind, V. Honkimäki, M. Daymond, *Nat. Mater.* 4 (2005) 33.
- [5] T.C. Hufnagel, R.T. Ott, J. Almer, *Phys. Rev. B* 73 (2006) 064204.
- [6] X.D. Wang, J. Bednarcik, K. Saksl, H. Franz, Q.P. Cao, J.Z. Jiang, *Appl. Phys. Lett.* 91 (2007) 081913.
- [7] M. Stoica, J. Das, J. Bednarcik, H. Franz, N. Mattern, W.H. Wang, J. Eckert, *J. Appl. Phys.* 104 (2008) 013522.
- [8] A.P. Hammersley, S.O. Svensson, M. Hanfland, A.N. Fitch, D. Häusermann, *High Press. Res.* 14 (1996) 235.
- [9] Y. Suzuki, T. Egami, *J. Non-Cryst. Solids* 75 (1985) 361.